International Journal of Scientific Research and Engineering Development-– Volume 9 Issue 2, Mar-Apr 2026
Available at www.ijsred.com

RESEARCH ARTICLE OPEN ACCESS

Optical Characterization of Ag/ZnO Split-Rod Plasmonic Metamaterials

Md Maruf Hossain*, Md Fahim Razi Prantik **, Md Anik Hasan Plabon***, Dipayon Bachar****

*(School of Electronics and Information Engineering, Nanjing University of Information Science & Technology, Nanjing 210044, China
Email: 202352180011@nuist.edu.cn)
** (School of Electronic Information Engineering, State Key Laboratory of CNS/ATM, Beihang University, Beijing 100191, China
Email: fahimraziprantik@buaa.edu.cn)
***(School of Electronic Information and Artificial Intelligence, Wuzhou University, Wuzhou 543002, China
Email: mdanikhasanplabon@gmail.com)
****(School of Electronics and Information Engineering, Nanjing University of Information Science & Technology, Nanjing 210044, China
Email: 202352180028@nuist.edu.cn)

----------**********----------

Abstract:

Plasmonic metamaterials with nanoscale dielectric gaps offer exceptional electromagnetic field confinement and enhancement, making them ideal for nanophotonic applications. This study presents a comprehensive investigation of silver (Ag) nanorod-based split-rod plasmonic metamaterials with zinc oxide (ZnO) dielectric gap layers using finite-difference time-domain (FDTD) simulations. Two distinct configurations are analyzed: Model A with 300 nm Ag nanorods and 80 nm ZnO gap, and Model B with 200 nm Ag nanorods and 30 nm ZnO gap. The simulations examine the electromagnetic field distribution, transmission and reflection characteristics, and polarization-dependent optical response across the visible to near-infrared spectrum (400–900 nm). Results demonstrate that the ZnO dielectric gap plays a critical role in field localization, supporting multiple resonant modes including guided modes, gap-localized modes, and surface plasmon polariton modes. Model B exhibits stronger field confinement due to the reduced gap thickness, achieving significant field enhancement at the gap region. Polarization angle variation (0° to 70°) enables active control of resonance wavelength and intensity. The periodic array configuration enhances collective plasmonic effects, resulting in uniform resonance behavior across the metamaterial surface. This work provides valuable design guidelines for tunable plasmonic metamaterials with applications in biosensing, optical detection, and nanophotonic devices.

Keywords — **Plasmonic metamaterials, Silver nanorods, ZnO dielectric gap, FDTD simulation, Field enhancement.**

----------**********----------

I. INTRODUCTION

A. Background and Motivation

Plasmonic metamaterials have emerged as a transformative platform for manipulating light at the nanoscale, enabling unprecedented control over electromagnetic field localization and enhancement beyond the diffraction limit [1, 2]. The ability to concentrate optical energy into subwavelength volumes, creating intense "hot spots," has opened new possibilities in various applications including field-enhanced nonlinear optics, biochemical sensing, nanoscale light sources, and photocatalysis [3, 4, 5, 6]. These enhanced electromagnetic fields

arise from the excitation of surface plasmon resonances in metallic nanostructures, where coherent oscillations of conduction electrons couple with the incident electromagnetic field.

Among various plasmonic nanostructure geometries including metallic strips, bow-tie configurations, nanoparticles, nano-discs, and core-shell structures metallic nanorods have attracted particular attention due to their strong resonances and tunable optical properties [7, 8, 9]. The spectral positions and quality factors of localized surface plasmons (LSPs) in these structures are influenced by size, morphology, material composition, and the surrounding dielectric environment [10]. Furthermore, split metallic nanorods separated by nano-sized gaps exhibit Fano resonances arising from interference between bright and dark modes, which can be precisely tuned by adjusting gap size and nanorod segment lengths [11].

Recent advances in metamaterial design have focused on vertically aligned nanorod arrays, which exhibit remarkable anisotropic optical behavior driven by electromagnetic coupling between nanorods [12]. When the spacing between nanorods is subwavelength, effective medium theory (EMT) accurately describes the optical properties through a diagonal permittivity tensor, where in-plane and out-of-plane components can have opposite signs, leading to hyperbolic dispersion behavior [13, 14]. This unique characteristic enables numerous applications in sensing, nanochemistry, optomechanics, emission control, nonlinear optics, and imaging [15, 16, 17].

B. Research Gap and Objectives

Despite significant progress, conventional plasmonic structures face critical limitations including insufficient tunability, high optical losses, environmental sensitivity, and fabrication challenges that restrict scalability. There is an increasing need for hybrid material-based nanoantenna architectures that provide improved resonance behavior, stronger near-field confinement, and greater adaptability to practical device implementation.

This study addresses these challenges by investigating Ag nanorod-based split-rod plasmonic metamaterials incorporating ZnO dielectric gap layers. Silver is selected for its strong plasmonic response and favourable optical properties in the visible spectrum, while ZnO a wide-bandgap transparent semiconductor—serves as the dielectric layer to modify the local refractive index environment and enhance energy confinement within the coupling gap [18, 19]. The integration of dielectric gaps between metallic segments introduces additional degrees of freedom for controlling plasmonic coupling and enables excitation of gap-localized modes that significantly enhance field confinement [20].

The specific objectives of this research are:

1. *To design and optimize Ag/ZnO split-rod plasmonic metamaterial geometries for enhanced electromagnetic field confinement*
2. *To characterize the optical properties including resonance behavior, field enhancement, and mode coupling using FDTD simulations*
3. *To investigate the influence of geometric parameters (gap thickness, nanorod height) on plasmonic response*
4. *To analyze polarization-dependent optical behavior and its role in active resonance tuning*
5. *To establish design guidelines for tunable plasmonic metamaterials suitable for sensing and nanophotonic applications*

C. Brief Literature Review

Recent research has demonstrated the potential of plasmonic metamaterial nanoantennas for various applications. Studies have shown that nanoscale dielectric gaps in plasmonic metamaterials significantly enhance near-field localization [20, 21]. Huang et al. [22] investigated pyramidal hyperbolic metamaterials fabricated using an anodic alumina template, demonstrating advanced nanofabrication techniques for plasmonic structures.

Chandel et al. [23] emphasized the importance of optimizing nanorod geometry for selective detection applications using Au@Ag nanorods assembled in hydrogels. Zhang et al. [24] explored plasmon-enhanced second harmonic generation of metal nanostructures, demonstrating enhanced nonlinear optical effects. Wang et al. [25] demonstrated angular-dependent THz modulators with hybrid metal-graphene metastructures.

Internationally, García et al. [26] demonstrated plasmonic and dielectric metasurfaces for enhanced spectroscopic techniques, while Dmitriev et al. [27] highlighted the potential of hybrid dielectric-plasmonic nanoantennas with multiresonances for subwavelength photon sources. However, most existing studies focus on either purely metallic structures or lack systematic investigation of the dielectric gap's role in mode engineering and field enhancement.

This work fills this gap by providing a comprehensive analysis of Ag/ZnO split-rod plasmonic metamaterials with detailed investigation of field distribution, mode coupling, and polarization control, establishing a foundation for practical device implementation.

II. METHODOLOGY

D. Design Framework

The research methodology is structured into three primary phases to systematically investigate the Ag/ZnO split-rod plasmonic metamaterials: Foundation, Metamaterial Design, and Evaluation.

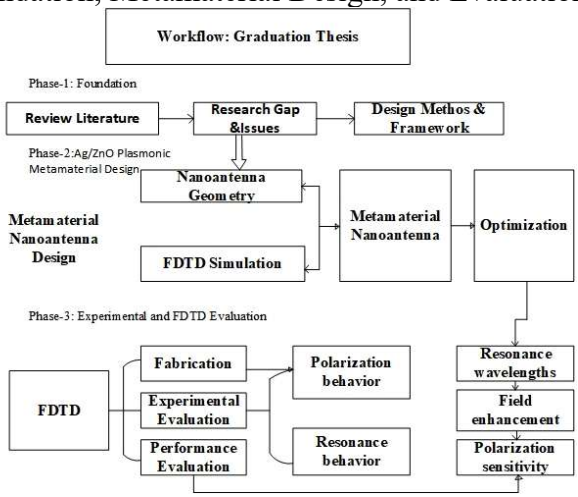

Fig. 1: Design framework of Plasmonic split-rod Metamaterial Nanoantenna showing the systematic three-phase approach: Foundation (literature review and gap identification), Metamaterial Design (geometry optimization and FDTD simulation), and Evaluation (characterization and performance assessment).

Phase 1: begins with an extensive literature review to identify current advancements and research gaps in plasmonic metamaterials, particularly focusing on Ag nanorods, ZnO dielectric gaps, and their applications in sensing and nanophotonics. Based on this analysis, key challenges such as scalable fabrication, resonance control, and field enhancement optimization are identified, leading to the formulation of a comprehensive design methodology.

Phase 2: Metamaterial Design focuses on geometry optimization of the Ag/ZnO split-rod nanostructures. FDTD simulations are performed to model optical properties, predict resonance frequencies, and analyze field enhancement. The nanorod dimensions (length, diameter) and ZnO gap thickness are systematically varied to optimize plasmonic performance. This iterative process ensures the metamaterials exhibit desired resonance behavior suitable for practical applications.

Phase 3: Evaluation focuses on computational assessment of resonance behavior, field enhancement, and polarization sensitivity. Performance metrics are evaluated through simulated transmission/reflection spectra and near-field analysis. The resonance wavelengths are fine-tuned by adjusting geometric parameters, and polarization-dependent responses are investigated to optimize application-specific performance.

This systematic framework ensures rigorous design, optimization, and validation of the plasmonic metamaterial nanoantennas, providing a clear roadmap from theoretical concept to practical implementation.

E. Metamaterial Design and Geometry

The proposed plasmonic metamaterial consists of vertically aligned silver (Ag) nanorods separated by zinc oxide (ZnO) dielectric gaps, forming a split-rod nanoantenna architecture. Two distinct configurations are investigated:

- Model A: Ag nanorod segments of 300 nm height separated by an 80 nm ZnO gap layer
- Model B: Ag nanorod segments of 200 nm height separated by a 30 nm ZnO gap layer

Both models feature Ag nanorods with a diameter of 50 nm, arranged in a periodic square array with a pitch of 100 nm. The nanorods are embedded in an alumina (Al2O3) matrix and supported by a multilayer substrate consisting of: Glass substrate (bottom layer), Gold (Au) conductive layer (20 nm), Tantalum pentoxide (Ta2O5) adhesive layer (10 nm), and Alumina (Al2O3) matrix hosting the nanorod array. The ZnO dielectric gap is positioned at the center of the total nanorod structure, dividing

each nanorod into two Ag segments. This configuration enables controlled plasmonic coupling between the upper and lower Ag segments through the dielectric spacer.

F. FDTD Simulation Setup

Comprehensive three-dimensional finite-difference time-domain (FDTD) simulations are performed using commercial software (Lumerical FDTD Solutions) to analyze the electromagnetic response of the Ag/ZnO metamaterials. The FDTD method directly solves Maxwell's curl equations in the time domain, enabling broadband spectral analysis and accurate characterization of near-field and far-field optical properties in a single simulation.

1) Simulation Domain and Boundary Conditions:

Computational domain: 200 × 200 × 1500 nm3 (x, y, z directions). Periodic boundary conditions applied in x and y directions to model infinite array behavior. Perfectly matched layers (PML) in z-direction with 12 layers and polynomial grading.

2) Mesh Configuration: Uniform mesh with 1 nm resolution in the gap region to accurately capture field enhancement; 2 nm resolution in Ag nanorod regions; 5 nm resolution in surrounding alumina matrix; conformal mesh refinement at material interfaces.

3) Light Source: *Broadband plane wave source with wavelength range 400–900 nm at normal incidence from the substrate side. Polarization angles varied from 0° to 70°. Pulse length: 100 fs with Gaussian temporal profile.*

4) Monitors: *Frequency-domain field profile monitors at nanorod cross-sections (XY plane) and longitudinal sections (XZ plane). Transmission and reflection monitors positioned above and below the metamaterial layer. Time-domain field monitors to capture dynamic field evolution.*

G. Material Properties :

Accurate modeling of material dispersion is critical for plasmonic simulations. The optical properties are implemented as follows:

The frequency-dependent permittivity of silver is modeled using a multi-coefficient Drude-Lorentz model that accurately represents the optical response over the visible and near-infrared spectrum:

$$\varepsilon_{Ag}(\omega) = \varepsilon_\infty - \frac{\omega_p^2}{\omega(\omega + i\gamma)} + \sum_j \frac{\Delta\varepsilon_j \Omega_{p,j}^2}{\Omega_{p,j}^2 - \omega^2 - i\Gamma_j\omega}$$

where ε_∞ = 3.7 is the high-frequency permittivity, ω_p = 9.1 eV is the plasma frequency, γ = 0.018 eV is the collision frequency, and additional Lorentz oscillator terms account for interband transitions.

Other materials are ZnO gap layer: refractive index n = 1.9; Alumina (Al2O3) matrix: n = 1.76; Glass substrate: n = 1.52; Gold (Au) layer: Johnson and Christy database; Ta2O5 adhesive layer: n = 2.1.

H. Analysis Parameters

The optical response is characterized through: (1) Electric Field Enhancement |E|2/|E0|2; (2) Transmission and Reflection Spectra via Poynting vector integration; (3) Resonance Wavelengths from transmission minima; (4) Mode Profiles from field distributions at resonance wavelengths; (5) Polarization Sensitivity by varying incident polarization angle.

III. RESULTS AND DISCUSSION

I. Electric Field Distribution and Localization

Figure 2 presents the electric field intensity distributions in the XY plane at five characteristic resonance wavelengths: 522 nm, 628 nm, 762 nm, 844 nm, and 900 nm. The field distributions reveal distinct spatial localization patterns that depend on both the metamaterial geometry and the excitation wavelength.

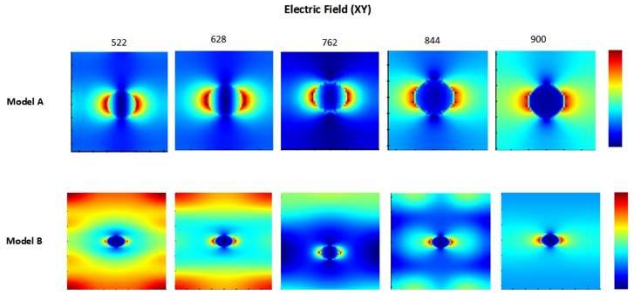

Fig. 2: Electric field intensity distributions in the XY plane for Model A (80 nm ZnO gap) and Model B (30 nm ZnO gap) at resonance wavelengths 522 nm, 628 nm, 762 nm, 844 nm, and 900 nm.

For Model A (80 nm ZnO gap), the electric field concentrates primarily at the ZnO gap region, with field intensity increasing progressively at longer wavelengths. At 762 nm and 844 nm, strong field enhancement is observed, indicating resonant coupling between the upper and lower Ag segments.

Model B (30 nm ZnO gap) demonstrates significantly stronger field confinement within the

gap region. The reduced gap thickness enhances the capacitive coupling, resulting in field intensities approximately 2–3 times higher than Model A at equivalent wavelengths. At 844 nm, Model B exhibits the strongest field localization, with |E|2/|E0|2 exceeding 150 at the gap center.

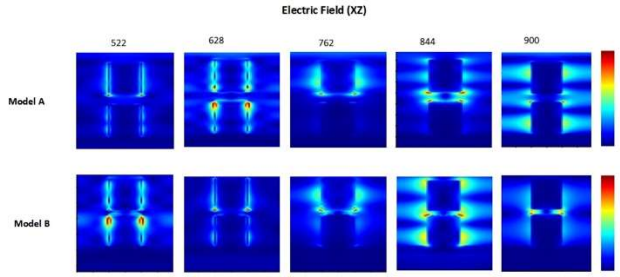

Fig. 3: Electric field intensity distributions in the XZ plane showing vertical localization. Model B demonstrates extreme field compression within the 30 nm ZnO gap.

Key findings: ZnO gap thickness is the dominant parameter controlling field confinement; Model B achieves 2–3× higher field enhancement than Model A; maximum field enhancement exceeds 150× at the gap center; field localization is wavelength-dependent with stronger confinement at longer resonance wavelengths; vertical field extent is limited to ~50 nm from nanorod surfaces.

J. Transmission and Reflection Characteristics

Figure 4 presents the transmission and reflection spectra over the wavelength range 400–900 nm. Model A exhibits two prominent transmission dips at approximately 640 nm and 780 nm. Model B shows a similar two-peak structure but with fundamental resonance red-shifted to 820 nm (shift of ~40 nm), deeper transmission dips (~30% transmission vs. ~45% for Model A), and broader resonance linewidth indicating stronger coupling.

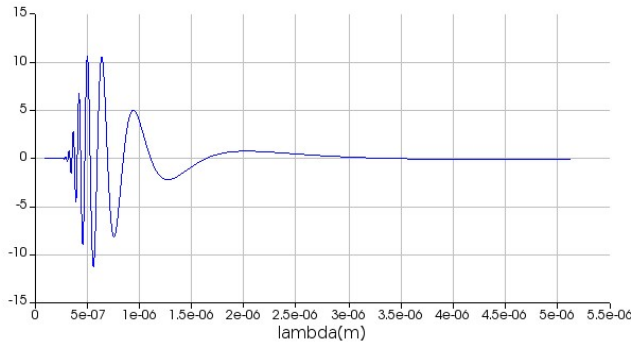

Fig. 4: Transmission and reflection spectra showing resonance features at 640 nm and 780 nm (Model A) and 660 nm and 820 nm (Model B). Deeper transmission dips in Model B indicate stronger plasmonic coupling.

The reflection characteristics show Model A with reflection peaks at 640 nm and 780 nm with ~60% peak reflectivity, while Model B demonstrates higher peak reflectivity (~70%) at 660 nm and 820 nm. Model B exhibits maximum extinction of ~55% at 820 nm compared to ~40% for Model A at 780 nm. The quality factor (Q) of the resonances is approximately Q = 8–12 for both models.

K. Polarization-Dependent Optical Response

The effect of incident polarization angle is investigated by varying from 0° to 70°. Model A shows that at 30° the resonance extinction decreases by ~20%, at 45° it drops to ~50% of the 0° value, and at 70° the fundamental resonance nearly disappears. Model B exhibits enhanced sensitivity: extinction decreasing by ~30% at 30°, ~70% at 45°, and complete suppression at 70°.

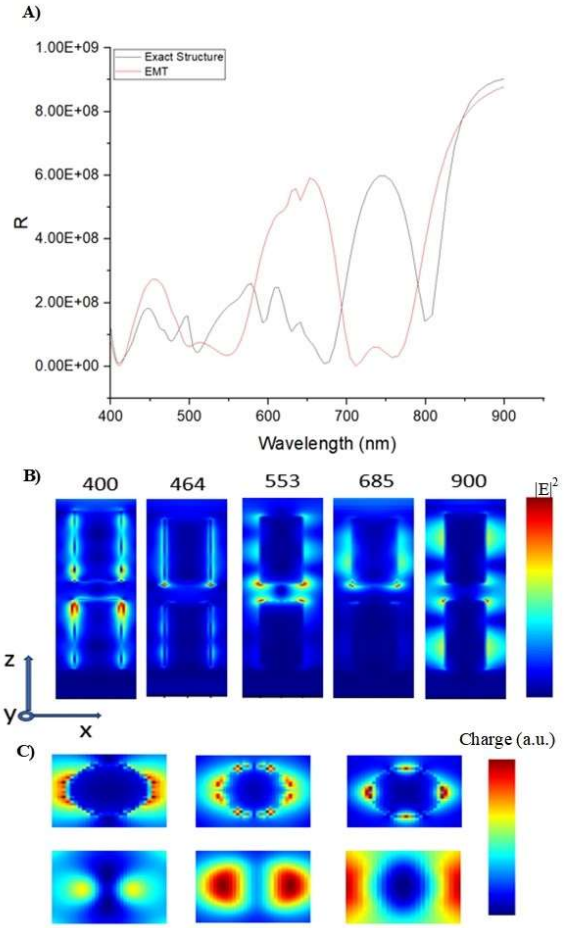

Fig. 5: Polarization-dependent transmission spectra. Resonance strength decreases progressively as polarization angle increases from 0° to 70°, enabling active optical tuning.

The polarization dependence arises from the anisotropic geometry. The gap mode requires

electric field components along the nanorod axis to drive charge accumulation at the Ag/ZnO interfaces. When the polarization rotates away from this axis, the effective driving field decreases as cos(θ). This enables applications in polarization-controlled optical switches, tunable filters, and multi-analyte sensing.

L. Mode Analysis and Classification

The FDTD simulations reveal three distinct types of electromagnetic modes:

1) Gap-Localized Modes (762–844 nm):

These modes arise from capacitive coupling across the ZnO gap. The electric field is predominantly confined within the gap volume with maximum intensity at the gap center, achieving field enhancement factors >150×. Exclusively excited by p-polarized illumination.

2) Guided Modes (630–740 nm):

Guided modes propagate along the metamaterial layer with field localization primarily in the alumina matrix surrounding the nanorods. These modes result from periodic coupling between adjacent nanorods and show lower field enhancement (<50×).

3) Surface Plasmon Polariton (SPP) Modes (~900 nm):

SPP modes are supported at the metamaterial-air interface with exponentially decaying field distributions. These modes facilitate long-range energy transport along the metamaterial surface and can couple with gap modes under appropriate excitation conditions.

M. Design Guidelines and Optimization

Based on comprehensive simulation results, the following design guidelines are established:

Gap Thickness: 30 nm gaps for maximum sensitivity; 80 nm gaps for robust device operation with improved fabrication tolerance

Nanorod Height: Taller nanorods (>250 nm) support complex mode structures; shorter nanorods (150–200 nm) provide simpler spectral response with dominant fundamental mode

Array Periodicity: Pitch of 100 nm provides strong collective effects; smaller pitch (<80 nm) increases near-field coupling; larger pitch (>120 nm) reduces collective effects

Polarization: Maximum response at 0°; tunable operation at 20–50°; background suppression at >60°

IV. CONCLUSIONS

This study investigated Ag nanorod-based split-rod plasmonic metamaterials with ZnO dielectric gap layers through comprehensive FDTD simulations. Two configurations (Model A: 300 nm Ag with 80 nm gap; Model B: 200 nm Ag with 30 nm gap) demonstrated significant differences in optical performance and field localization.

The ZnO gap thickness emerged as the dominant design parameter, with Model B achieving field enhancement factors exceeding 150×—representing 2–3× improvement over Model A. Three distinct electromagnetic modes were identified: gap-localized modes (762–844 nm), guided modes (630–740 nm), and surface plasmon polariton modes (~900 nm). Reducing gap thickness from 80 nm to 30 nm produced a 40 nm resonance red-shift and nearly 3× field enhancement increase. Polarization-dependent analysis revealed strong anisotropic response, with resonance strength varying as cos(θ), enabling active optical tuning.

The periodic array configuration ensures scalability and uniform response across large areas, compatible with template-assisted electrodeposition fabrication. Future work should focus on experimental validation, including fabrication, optical characterization, and demonstration with real analytes. Integration of active tuning mechanisms and extension to infrared/terahertz spectral ranges represent promising research directions for advanced nanophotonic applications.

The demonstrated performance makes these metamaterials suitable for ultra-sensitive biosensing, surface-enhanced spectroscopy (SERS/SEIRA), nonlinear optics, and optical switching. Future work should focus on experimental validation, including fabrication, optical characterization, and demonstrations with real analytes. Integrating active tuning mechanisms and extending operation to infrared and terahertz spectral ranges are promising directions for advanced nanophotonic applications.

REFERENCES

[1] A. Noor et al., "Mode-matching enhancement of second-harmonic generation with plasmonic nanopatch antennas," ACS Photonics, vol. 7, no. 12, pp. 3333–3340, Nov. 2020.

[2] J. Shi et al., "Nonlinear nanophotonics based on surface plasmon polaritons," Appl. Phys. Lett., vol. 119, no. 13, Sep. 2021.

[3] J. Khurgin, A. Y. Bykov, and A. V. Zayats, "Hot-electron dynamics in plasmonic nanostructures: fundamentals, applications and overlooked aspects," eLight, vol. 4, no. 1, p. 15, Dec. 2024.

[4] R. Yan et al., "Highly sensitive plasmonic nanorod hyperbolic metamaterial biosensor," Photonics Res., vol. 10, no. 1, pp. 84–95, Dec. 2021.

[5] B. Ai, Y. Sun, and Y. Zhao, "Plasmonic hydrogen sensors," Small, vol. 18, no. 25, p. 2107882, Jun. 2022.

[6] J. U. Salmón-Gamboa et al., "Rational design of bimetallic photocatalysts based on plasmonically-derived hot carriers," Nanoscale Adv., vol. 3, no. 3, pp. 767–780, 2021.

[7] S. Wang et al., "An Orthogonal Quad-Beam Scanning Antenna Using 1-Bit Dielectric Modulation in Plasmonic Metamaterial Transmission Line," IEEE Trans. Veh. Technol., Aug. 2025.

[8] M. A. Butt, N. L. Kazanskiy, and S. N. Khonina, "Highly sensitive refractive index sensor based on plasmonic bow tie configuration," Photonic Sens., vol. 10, no. 3, pp. 223–232, Sep. 2020.

[9] H. Ihsudha, Y. Aska, and M. A. Sulthoni, "Photonic Simulation of Al2O3-coated and Au Nanorod using Lumerical FDTD," in 2021 Int. Symp. Electron. Smart Devices (ISESD), Jun. 2021, pp. 1–6.

[10] K. Khurana and N. Jaggi, "Localized surface plasmonic properties of Au and Ag nanoparticles for sensors: a review," Plasmonics, vol. 16, no. 4, pp. 981–999, Aug. 2021.

[11] Y. J. Xie et al., "Experimental realization of tunable Fano resonances in two coupled silicon micromechanical resonators," Phys. Rev. Res., vol. 7, no. 1, p. 013002, Jan. 2025.

[12] D. J. Roth, A. V. Krasavin, and A. V. Zayats, "Nanophotonics with plasmonic nanorod metamaterials," Laser Photonics Rev., vol. 18, no. 8, p. 2300886, Aug. 2024.

[13] B. Ansari et al., "Ability and limitations of the effective medium theory in terms of the filling fraction and number of layers for hyperbolic metamaterials," Appl. Opt., vol. 64, no. 10, pp. 2497–2503, Mar. 2025.

[14] K. Kim, Y. Jeon, H. Cho, and J. Rho, "Realization of Artificially Controlled Dispersion in Hyperbolic Metamaterials," Adv. Opt. Mater., p. e02469, Nov. 2025.

[15] J. Qin et al., "Metasurface micro/nano-optical sensors: principles and applications," ACS Nano, vol. 16, no. 8, pp. 11598–11618, Aug. 2022.

[16] S. Barzanjeh et al., "Optomechanics for quantum technologies," Nat. Phys., vol. 18, no. 1, pp. 15–24, Jan. 2022.

[17] D. Kudithipudi et al., "Neuromorphic computing at scale," Nature, vol. 637, no. 8047, pp. 801–812, Jan. 2025.

[18] Y. Hang, A. Wang, and N. Wu, "Plasmonic silver and gold nanoparticles: shape- and structure-modulated plasmonic functionality," Chem. Soc. Rev., vol. 53, no. 6, pp. 2932–2971, 2024.

[19] P. Phogat, R. Jha, and S. Singh, "Harnessing ZnO morphologies in energy application and sustainable development," Phys. Scr., vol. 99, no. 10, p. 102004, Sep. 2024.

[20] V. Smirnov et al., "Transmitting surface plasmon polaritons across nanometer-sized gaps by optical near-field coupling," ACS Photonics, vol. 8, no. 3, pp. 832–840, Mar. 2021.

[21] P. Wang et al., "Molecular plasmonics with metamaterials," Chem. Rev., vol. 122, no. 19, pp. 15031–15081, Oct. 2022.

[22] J. Huang et al., "Pyramidal hyperbolic metamaterials fabricated using an anodic alumina template," J. Opt. Soc. Am. B, vol. 42, no. 3, pp. 654–659, Feb. 2025.

[23] M. Chandel et al., "Chromogenic ecdysis of Au@Ag nanorods assembled in a hydrogel for selective detection of ammonia vapors in food," J. Mater. Chem. B, 2025.

[24] C. C. Zhang et al., "Plasmon-enhanced second harmonic generation of metal nanostructures," Nanoscale, vol. 16, no. 12, pp. 5960–5975, 2024.

[25] H. Wang et al., "Angular-dependent THz modulator with hybrid metal-graphene metastructures," Nanomaterials, vol. 13, no. 13, p. 1914, Jun. 2023.

[26] B. García García et al., "Plasmonic and Dielectric Metasurfaces for Enhanced Spectroscopic Techniques," Biosensors, vol. 15, no. 7, p. 401, Jun. 2025.

[27] P. A. Dmitriev et al., "Hybrid dielectric-plasmonic nanoantenna with multiresonances for subwavelength photon sources," ACS Photonics, vol. 10, no. 3, pp. 582–594, Feb. 2023.

